water

MDPI

Article

Risk Assessment of Urban Water and Energy Supply Using Copula Function: A Water–Energy Nexus Approach in an Arid City

Mohammad Reza Goodarzi [1,2,*], Maryam Sabaghzadeh [3], Samane Al-sadat Mousavi [4] and Majid Niazkar [5,6,*]

[1] Department of Civil Engineering, Faulty of Engineering, Ferdowsi University of Mashhad, Mashhad 9177948974, Iran
[2] Department of Civil Engineering, Yazd University, Yazd 8915813135, Iran
[3] Department of Civil Engineering, Water Resources Management Engineering, Yazd University, Yazd 8915813135, Iran
[4] Department of Statistics, College of Mathematics, Yazd University, Yazd P.O. Box 89195-741, Iran
[5] Euro-Mediterranean Center on Climate Change, Porta dell'Innovazione Building, 2nd Floor Via della Libertà, 12, Marghera, 30175 Venice, Italy
[6] Porta dell'Innovazione Building, Ca' Foscari University of Venice, 2nd Floor Via della Libertà, 12, Marghera, 30175 Venice, Italy
* Correspondence: goodarzimr@um.ac.ir or goodarzimr@yazd.ac.ir (M.R.G.); majid.niazkar@cmcc.it or majid.niazkar@unive.it (M.N.)

Abstract: Planning for the future of water and energy supply systems in urban areas requires a thorough assessment of associated risks. In this study, monthly water and energy demand data from 2011 to 2022 in an arid city was used to predict the corresponding demands from 2023 to 2032 using the seasonal auto-regressive integrated moving average (SARIMA) method. The aim is to estimate future water and energy supply risks both individually and jointly, using cumulative distribution functions (CDFs) derived from historical data. The main focus is to calculate the combined risk of water and energy, referred to as the water–energy nexus (WEN) risk. Based on the interdependent relationship between water and energy, the Copula function was utilized to model the bivariate distribution between these two variables. Pearson correlation analysis indicated a strong correlation between water and energy supplies. Among the distributions fitted to the data, the log-normal and gamma distributions were the best fit for water supply and energy supply systems, respectively, with the lowest Akaike information criterion (AIC) values. The Gumbel Copula, with a parameter of 1.66, was identified as the most suitable for modeling the joint distribution, yielding the lowest AIC value. The results indicate that the risks associated with energy supply, water supply, and their joint dependency could exceed 0.8% in the future, highlighting a potentially critical situation for the city. The trend analysis revealed that forecasted water and energy demands and their corresponding risks and the WEN risk are expected to have a significant upward trend in the future. Finally, local authorities need to explore alternative sources to supply water and energy in the future to address the ever-growing water and energy demands.

Keywords: water–energy nexus; water demand; energy demand; risk; copula function; SARIMA

check for updates

Citation: Goodarzi, M.R.; Sabaghzadeh, M.; Mousavi, S.A.-s.; Niazkar, M. Risk Assessment of Urban Water and Energy Supply Using Copula Function: A Water–Energy Nexus Approach in an Arid City. *Water* **2024**, *16*, 3077. https://doi.org/10.3390/w16213077

Academic Editor: Robert Sitzenfrei

Received: 27 September 2024
Revised: 22 October 2024
Accepted: 25 October 2024
Published: 27 October 2024

Copyright: © 2024 by the authors. Licensee MDPI, Basel, Switzerland. This article is an open access article distributed under the terms and conditions of the Creative Commons Attribution (CC BY) license (https://creativecommons.org/licenses/by/4.0/).

1. Introduction

Humans have always sought ways to meet their essential needs, such as water and energy demands. Water is one of the most critical resources, as securing its supply has been a constant effort throughout human history [1]. This issue is particularly challenging in regions with hot and arid climates, where low rainfall patterns prevail [2]. Historically, the water supply in arid areas relied solely on groundwater, while excessive groundwater extraction over time has led to additional problems, such as land subsidence [3]. As a result, in these regions, seeking alternative solutions to secure water needs is crucial. In recent

years, strategies, such as water transfer and the treatment and reuse of wastewater, have been explored to help meet the water demands of arid regions [4].

In addition to water supply, energy provision is a fundamental necessity, particularly in urban areas. Nowadays, cities cannot function without energy and electricity; thus, it is important for water utilities and authorities to ensure that the energy supply system is steady [5]. This challenge becomes more severe during the summer months in hot regions, when rising temperatures increase energy consumption, complicating its supply [6]. Since energy consumption often depends on water availability, water shortages can consequently impact energy supply. Therefore, a more comprehensive analysis can be conducted if water and energy are considered together. This concept, known as nexus, has been the focus of many studies since 2011 [7].

The nexus suggests that considering essential human needs, such as water, energy, food, environment, and economy, altogether can lead to optimized resource allocation and sustainable future development [8]. Various models have been used for risk assessment in urban water and energy systems. Bayesian networks model uncertainties and perform scenario analysis, while system dynamics models simulate complex feedback relationships over time [9,10]. Multi-objective optimization models allocate resources and assess risks based on different scenarios, and Monte Carlo simulations evaluate risks by generating random samples for uncertain variables like demand and climate variability [11,12].

In addition to addressing the current needs of a region, authorities should account for future changes as well. By predicting future consumption patterns and potential resource shortages, they can make more informed decisions regarding the management of water and energy resources. This approach not only allows for proactive planning but also helps mitigate the impacts of anticipated challenges, ensuring sustainable management of water and energy resources [13].

To date, numerous studies have been conducted on water and energy supply systems, as well as the associated risks and future predictions [14–16]. For instance, Chen et al. [17] developed multidimensional models to improve water resource utilization, hydropower generation, and environmental impacts. Considering the joint distributions among the variables in the Yangtze River basin, their models showed that the excessive production of hydropower energy can lead to water shortages and environmental damage upstream. Furthermore, Chen et al. [18] developed an optimization model considering the water–energy nexus (WEN) to handle uncertain and fuzzy parameters. Their results indicated that the use of fossil fuels has a large contribution to the carbon production of the region, while the implementation of policies, such as a carbon tax, can reduce carbon emissions even though it increases system costs. Cai et al. [19] used Markov and Copula chains to design a model for water and energy management in the North China region. Their findings demonstrated that the risks related to energy, especially under conditions of multiple pressures, are more severe than the risks of water. Alnahhal et al. [20] used water and energy coupling to optimize electricity and water systems. Their results showed that desalination techniques and water reservoirs can reduce operating costs. Kang et al. [21] implemented an integrated WEN assessment and forecasting approach in Mongolia and found that WEN has been consistently significant over time.

Despite valuable studies, key gaps still remain. In particular, many previous studies have only investigated interactions in specific regions, and their results may not apply to other regions with different characteristics, especially in arid and semi-arid regions. Furthermore, existing models have generally considered short-term impacts, and less attention has been paid to the long-term sustainability of resources and climate change. Also, many existing studies have limited focus on the comprehensive analysis of risks, as there is a need for multivariate analyses and the application of probabilistic models and system dynamics in different conditions.

Unlike previous studies that primarily focused on historical data or examined water and energy risks separately, this study calculated the risk of the water–energy nexus (WEN) in addition to evaluating the risk of water and energy supply separately. A probabilistic

model, i.e., the copula function, was exploited to assess the combined risk of water and energy supply within WEN. Due to the importance of water in dry areas, Yazd city in Iran, which has a hot and dry climate, was selected; no similar study has been conducted in this city. Furthermore, monthly data from 12 years (2011–2022) were considered in this study. Unlike most previous studies that mostly focused on the analysis of past data, the current study predicted water and energy demands and the risk of water and energy supply for the next 10 years.

2. Materials and Methods

2.1. Study Area

The city of Yazd, covering an area of 99.5 km^2, is in the center of Yazd province along the Esfahan-Kerman route and on the edge of Iran's central desert (Figure 1). Yazd has a dry, desert climate with a population of approximately 671,561 in 2016. It is the most populous city in the province [22]. Due to low rainfall (an average of 60 mm) and high evaporation rates (4 m/year), groundwater resources serve as the primary water supply for the city [23]. However, the declining groundwater levels and restrictions on extraction from the province plains have made it necessary to implement water transfer projects outside the province. Projects, including the transfer of water from the Zayandeh Rud and Beheshtabad rivers, desalination of water from the Persian Gulf, and the reuse of treated wastewater, are among the measures taken to ensure Yazd's water supply [24]. Additionally, the Yazd electricity is supplied by combined cycle and gas power plants, which also consume water, underscoring the WEN importance in the region [25]. It has consistently faced water and energy shortages, particularly during consumption peaks in the summer. Finally, monthly water and energy consumption data from 2011 to 2022 in Yazd were utilized.

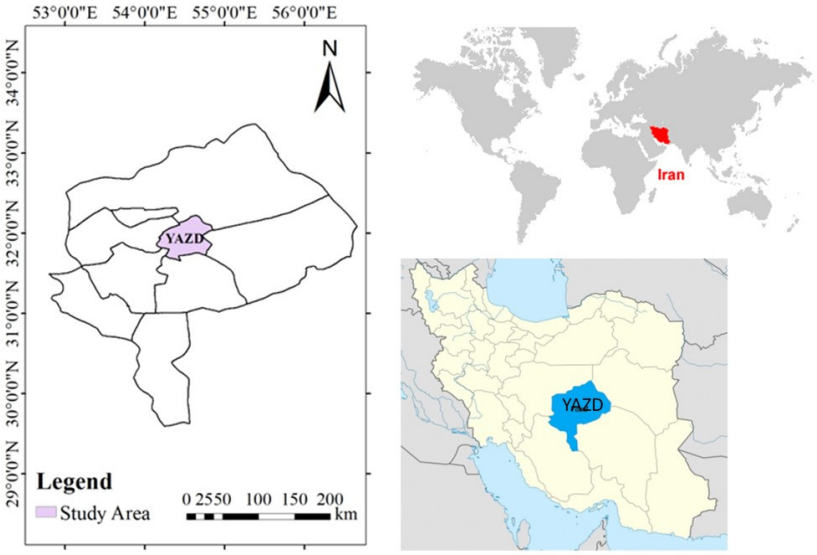


Figure 1. Location of Yazd (the red and purple show Iran and Yazd, respectively).

Monthly water and energy supply and demand data of Yazd were obtained from 2011 to 2022 from the Yazd Water and Electricity Organization. Water supply data include groundwater and transfer water, while energy supply data are the energy received from gas power plants and combined cycles. Additionally, the water and energy demands indicate the consumption of water and energy in the city.

Table 1 summarizes the statistical characteristics of the water and energy supply data. As shown, the water and energy supply data are slightly right-skewed. Furthermore, they have a lower kurtosis than a normal distribution and exhibit lighter tails. Also, water demand has a very low skewness, close to zero, while it has a higher kurtosis than a normal distribution. On the other hand, the energy demand has a positive skewness, and its kurtosis is close to a normal distribution.

Table 1. Summary of statistical properties of the data used in this study.

Data	Minimum	Maximum	Mean	Median	Standard Deviation	Skewness	Kurtosis
Water supply (million m^3)	1.152	7.537	4.703	4.479	1.204	0.38	−0.45
Energy supply (million MWh)	0.132	0.678	0.376	0.356	0.139	0.26	−1.02
Water demand (million m^3)	0.731	8.056	3.974	3.876	1.268	0.17	0.32
Energy demand (million MWh)	0.18	0.88	0.407	0.386	0.16	0.73	−0.08

2.2. Water–Energy Nexus

WEN is the complex and interdependent relationship between water resources and energy production and consumption. They are highly interconnected; for example, energy production requires substantial amounts of water, e.g., in hydroelectric and thermal power plants [26]. Any changes in water availability can directly impact energy production and vice versa. This nexus is particularly significant in the regions facing natural resource scarcity, while mismanagement can increase environmental and economic risks.

WEN highlights the interconnectedness between water resources and energy production. The latter often requires significant water, while water management relies heavily on energy for extraction and treatment. Disruptions in water availability, such as droughts, can directly affect energy production, particularly in water-intensive sectors [27]. Conversely, energy shortages can limit water extraction and distribution [28].

In arid regions like Yazd, the effective management of both resources is essential due to their scarcity. Changes in water availability can have substantial impacts on energy production, especially during peak demand periods, making integrated resource management crucial for minimizing risks and ensuring sustainable supply.

In Yazd, there are two types of power plants for electricity generation: combined cycle and gas power plants [29]. Water consumption of combined cycle power plants can vary depending on the type of cooling system (wet, dry, or hybrid) and the geographical location of the plant:

- Plants with wet cooling systems typically consume about 2000 to 3500 L of water per megawatt-hour (MWh).
- Plants with dry cooling systems use significantly less water, usually consuming less than 100 L per MWh.
- Water consumption of plants with hybrid cooling systems falls between those of wet and dry systems [30].

The combined cycle power plant in Yazd includes two gas turbines, each with a capacity of 162 MW, and one steam turbine with a capacity of 160 MW. The total capacity of the power plant is 484 MW, and the cooling towers are of the dry type.

Gas power plants also consume water, while their water consumption is generally lower than that of combined cycle or steam power plants. The amount and type of water consumption in gas power plants depend on the following factors:

- If a wet cooling system is used, approximately 300 to 750 L of water are consumed per MWh.
- Water consumption in a dry cooling system is less than 100 L per MWh.
- In hybrid systems, water consumption falls between 100 and 300 L per MWh.

In gas power plants with dry cooling systems, water consumption is significantly lower and is mainly limited to other processes [31]. The gas power plant in Yazd is a dry cooling system.

2.3. Time Series Forecasting Using SARIMA

The ARIMA method is one of the most widely used approaches for forecasting time series data. It includes three main components: (i) auto regressive (AR), (ii) integrated (I), and (iii) moving average (MA). The ARIMA model is generally represented as $ARIMA(p,\ d,\ q)$, where p is the non-seasonal autoregressive order, d is the degree of differencing needed to make the data stationary, and q denotes the non-seasonal moving average order [32]. The general formula for the ARIMA model is as follows:

$$\varphi(B)(\nabla)^d z_t = \theta(B)\varepsilon_t \tag{1}$$

Given the following relationship, the above equation can be rewritten as:

$$\nabla = (1 - B) \tag{2}$$

$$\varphi(B)(1 - B)^d z_t = \theta(B)\varepsilon_t \tag{3}$$

$$\varphi(B) = 1 - \varphi_1 B - \varphi_2 B^2 - \cdots - \varphi_P B^P \tag{4}$$

$$\theta(B) = 1 - \theta_1 B - \theta_2 B^2 - \cdots - \theta_q B^q \tag{5}$$

where B is a backward operator that acts on the time index and moves back by one time unit and obtains a new series, ∇ represents the differentiation of time series, $\varphi(B)$ is the autocorrelation (AR) part of the model, $\theta(B)$ is the moving average (MA) part, ε_t is a random noise or model error at time t, φ is the parameter of the non-seasonal autoregressive model, and θ is the parameter of the non-seasonal moving average model [33].

Differencing is used to achieve stationary in a time series. In this process, the data are differenced d times, and then the ARIMA model is applied to the stationary data.

In the selection process of the ARIMA model, the time series is first made stationary through differencing, then suitable values for the parameters p and q are determined using autocorrelation function (ACF) and partial autocorrelation function (PACF) plots [34].

If a time series exhibits seasonal trends, the ARIMA model extends to the Seasonal ARIMA (SARIMA) model to effectively account for seasonal prediction patterns. The SARIMA model adds seasonal components to ARIMA, allowing for the modeling of seasonal periods. It is represented as $SARIMA(p,\ d,\ q)(P, D, Q)_w$, where P, D, and Q represent the seasonal autoregressive order, seasonal differencing degree, and seasonal moving average order, respectively, and w is the number of seasonal periods in a year, e.g., 12 for monthly data [35].

SARIMA models are derived using the seasonal differencing operator with lag and are represented as $ARIMA(P, D, Q)_w$. To distinguish the seasonal model from the non-seasonal one, all letters in the notation are written in uppercase. The general form of the SARIMA model is as follows:

$$\varphi(B^\omega)(1 - B^\omega)^D z_t = \theta(B^\omega)\varepsilon_t \tag{6}$$

$$\varphi(B^\omega) = 1 - \varphi_1 B^\omega - \varphi_2 B^{2\omega} - \cdots - \varphi_p B^{p\omega} \tag{7}$$

$$\theta(B^\omega) = 1 - \theta_1 B^\omega - \theta_2 B^{2\omega} - \cdots - \theta_Q B^{Q\omega} \tag{8}$$

In the SARIMA model, the data are first made stationary through seasonal differencing (D) to remove seasonal trends. The ARIMA model is then applied to the seasonally adjusted data, with seasonal components incorporated using seasonal operators. This approach allows the model to capture both short-term patterns and long-term seasonal patterns, which significantly improves the accuracy of forecasts for seasonal time series [36].

2.4. Copula

2.4.1. Copula Structure

The interaction effect between water supply and energy supply relies on the univariate distributions of each and the dependence between them, which can be expressed through a Copula function. The Copula function links univariate distribution functions to form a multivariate distribution function [37]. Additionally, it can separate the marginal distribution from the dependency structure of a multivariate distribution [38]. Thus, the information in the copula includes all univariate information and the relationship between the variables.

According to Sklar's theorem, if the continuous random variables X and Y have marginal distribution functions $F(X)$ and (Y), respectively, and a joint distribution function $H(X, Y)$, the unique copula $C(u, v)$ is defined in Equation (9) [39]:

$$H(x, y) = C(F(x), G(y)) \tag{9}$$

Therefore, for the variables of water supply and energy supply with marginal distributions $F(X)$ and (Y), respectively, and the copula C, the joint distribution function can be obtained using Equation (9).

Using the copula function and Sklar's theorem is beneficial when there is a relationship between the variables. The Pearson correlation coefficient is a standard measure used to calculate the degree of dependence between two variables X and Y, and is computed in Equation (10) [40]:

$$r = \frac{cov(X, Y)}{\sqrt{var(X)}\sqrt{var(Y)}} \tag{10}$$

where $var(X)$ represents the variance of variable X and $cov(X, Y)$ indicates the covariance between variables X and Y.

To calculate the dependence between variables in the general cases (when nonlinear relationships are also considered), some non-parametric measures such as Kendall's tau and Spearman's rho are used. If X and Y are continuous random variables with corresponding Copula C, then Kendall's tau measure of dependence for X and Y is given in Equation (11):

$$\tau = 4\int_0^1 \int_0^1 C(u, v)dC(u, v) - 1 \tag{11}$$

The Spearman's rho measure of dependence (ρ) is calculated using Equation (12):

$$\rho = 12\int_0^1 \int_0^1 C(u, v)dudv - 3 \tag{12}$$

2.4.2. Selection of an Appropriate Copula Structure

To determine the appropriate copula structure, suitable marginal distributions for the water supply and energy supply variables need to be fitted. For fitting an appropriate marginal distribution for each data series, the Kolmogorov–Smirnov (KS) goodness-of-fit statistic, Akaike information criterion (AIC), log-likelihood, and the p-value of the Kolmogorov–Smirnov test are evaluated. The null hypothesis in goodness-of-fit tests is that the random variable X follows a distribution $F(X)$. This test uses the distance between the empirical distribution function and the estimated distribution function (under the null hypothesis) to assess whether the fitted distribution is appropriate.

The empirical distribution function ($F_n(X)$) is expressed as:

$$F_n(x) = \frac{1}{n}\sum_{i=1}^{n} I(X_i \leq x) \tag{13}$$

The estimated distribution function under the null hypothesis ($\hat{F}(x)$), the KS test is defined as follows [41]:

$$KS = sup_x\left|F_n(x) - \hat{F}(x)\right| \tag{14}$$

The smaller KS is, the better the distribution fits.

The log-likelihood statistic indicates how well the model with optimized parameters fits the data. For a sample of size n, with θ as the distribution parameter and $f(x_i|\theta)$ as the density function of the variable x_i with parameter θ, the log-likelihood function is defined as follows:

$$l(\theta|x_1, \ldots, x_n) = \sum_{i=1}^{n} \ln(f(x_i|\theta)) \quad (15)$$

Higher values of the log-likelihood function indicate that it provides a better fit to the data compared to other functions.

Finally, AIC seeks a function that describes the data well while avoiding unnecessary complexity. Distributions with a smaller AIC are considered better distributions [42]. It is defined using $l(\theta|x_1, \ldots, x_n)$ or, briefly, $l(\theta)$, as follows:

$$AIC = -2l(\theta) + 2k \quad (16)$$

where k is the number of parameters.

After determining suitable marginal distributions, the data are first transformed into uniform distributions using the probability integral transform theorem to model the dependency structure between the variables. Afterwards, the appropriate copula structure is identified [43]. This study considers some famous and widely used families, including elliptical copulas (normal and t-student) and Archimedean copulas (Gumbel, Frank, and Clayton). To determine the appropriate copula structure, the Cramér–von Mises goodness-of-fit test, AIC, log-likelihood, and p-value of the Cramér–von Mises test were used. In the Cramér–von Mises test, the null hypothesis is that the relationship between the variables follows a specific copula C. It is similar to the goodness-of-fit test for univariate distributions [44]. The empirical copula (C_n) is expressed in Equation (17):

$$C_n(u, v) = \frac{1}{n} \sum_{i=1}^{n} I\left(F(x_i) \leq u\ ,\ G(y_i) \leq v\right) \text{ for } u, v\ \epsilon[0, 1] \quad (17)$$

where $F(x_i)$ and $G(y_i)$ are the marginal distributions of X and Y, respectively.

The Cramér–von Mises test is a function of the distance between the empirical copula and the estimated copula under the null hypothesis $C_{\hat{\theta}}(u, v)$. It is derived from Equation (18):

$$S_n = \int_0^1 \int_0^1 \left(\sqrt{n}\left(C_n(u, v) - C_{\hat{\theta}}(u, v)\right)\right)^2 dC_n(u, v) \quad (18)$$

where $C_n(u, v)$ is the empirical copula, and $C_{\hat{\theta}}(u, v)$ is the estimated copula under the null hypothesis.

Large values of the S_n statistic indicate a rejection of the null hypothesis.

2.5. Trend Analysis Method

Mann–Kendall's test is a non-parametric trend analysis method. It has been widely used for trend detection for hydroclimatic data series [45]. Its primary advantages are (i) being less affected by extreme values and (ii) no reliance on a specific statistical distribution. In this technique, the standardized statistic of Mann–Kendall's test (Z) is used to identify the presence of a trend in a data series [46]:

$$Z = \begin{cases} \frac{S-1}{\sqrt{Var(S)}} & S > 0 \\ 0 & S = 0 \\ \frac{S+1}{\sqrt{Var(S)}} & S < 0 \end{cases} \quad (19)$$

where S is Mann–Kendall's static test and can be obtained by Equation (20):

$$S = \sum_{i=1}^{n-1} \sum_{j=i+1}^{n} sgn\left(x_j - x_i\right) \quad (20)$$

where $sgn(x_j - x_i) = \begin{cases} 1 & x_j > x_i \\ 0 & x_j = x_i \\ -1 & x_j < x_i \end{cases}$.

If $|Z| > 0.96$, the null hypothesis, which implies no trend in the data series, is rejected. Otherwise, the alternative hypothesis, which suggests the presence of a statistically significant trend, is accepted. Furthermore, a positive Z typically indicates an increasing trend, whereas a negative Z means a negative trend. Therefore, based on Z in Mann–Kendall's test, the existence and magnitude of a trend can be examined in the data series.

2.6. Performance Evaluation Indices

The results obtained in this study were evaluated using four metrics. These metrics are commonly used to evaluate the performance of forecasting models and timing in statistical analyses and time series predictions [47,48]:

1. Mean error (*ME*): *ME* refers to the average difference between the predicted values and the actual values (Equation (21)). It can be either positive or negative, indicating the bias of the forecasting system. A negative value indicates that the model predicted slightly less than the actual value on average. In contrast, a positive value implies that the model estimated slightly more than the actual value. Thus, the closer ME to zero is, the better the model performs:

$$ME = \frac{1}{n}\sum_{i=1}^{n}(o_i - p_i) \tag{21}$$

where o_i and p_i are the ith observed and predicted values, respectively, and n is the sample size.

2. Root mean squared error (*RMSE*): *RMSE* indicates the degree of deviation of the predictions from the actual values (Equation (22)). It is highly sensitive to significant errors and is expressed in the same units as the data:

$$RMSE = \sqrt{\frac{1}{n}\sum_{i=1}^{n}(o_i - p_i)^2} \tag{22}$$

3. Mean absolute scaled error (*MASE*): *MASE* is used to compare model performances with baseline data by scaling the absolute error achieved by the model relative to a baseline model:

$$MASE = \frac{\frac{1}{n}\sum_{i=1}^{n}|(o_i - p_i)|}{\frac{1}{n-1}\sum_{i=2}^{n}|(o_i - o_{i-1})|} \tag{23}$$

4. Nash–Sutcliffe efficiency (*NSE*): *NSE* has been widely used in environmental and hydrological sciences to evaluate how well hydrological models or other forecasting models perform in replicating observed events by comparing observed data to predicted data:

$$NSE = 1 - \frac{\sum_{i=1}^{n}(o_i - p_i)^2}{\sum_{i=1}^{n}(o_i - \overline{o})^2} \tag{24}$$

where $\overline{o}$ is the mean of the observed values.

5. Determination coefficient (R^2): It is a statistical measure representing the proportion of the variance in the dependent variable (observed data) that is predictable from the independent variable (predicted data):

$$R^2 = \frac{\left[\sum_1^n (o_i - \overline{o}_i)(p_i - \overline{p})\right]^2}{\sum_1^n (o_i - \overline{o}\,)^2 . \sum_1^n (p_i - \overline{p})^2} \tag{25}$$

where $\overline{p}$ is the mean of the predicted values.

3. Results

3.1. Time Series Forecasting with SARIMA

SARIMA was used to forecast the water and energy supply. Despite its simplicity, it can effectively match observational data and forecast future values if the time series does not have significant complexity. After separating the components of each series, it was observed that both have seasonal trends. Consequently, SARIMA was used to model and forecast water and energy supply for Yazd.

Various SARIMA models were applied to the data, and finally, SARIMA(5,2,3)$(2,1,3)_{12}$ and SARIMA(2,1,2)$(1,2,2)_{12}$ were selected for water demand and electricity demand. Figure 2 depicts the forecasted water demand in millions of cubic meters (million m^3) and energy demands in million megawatt-hours (million MWh) from 2011 to 2022 in Yazd. As shown, the comparison of observed and predicted demands indicates that the SARIMA models have effectively predicted water and energy demand as they adequately captured the patterns of the available historical data.

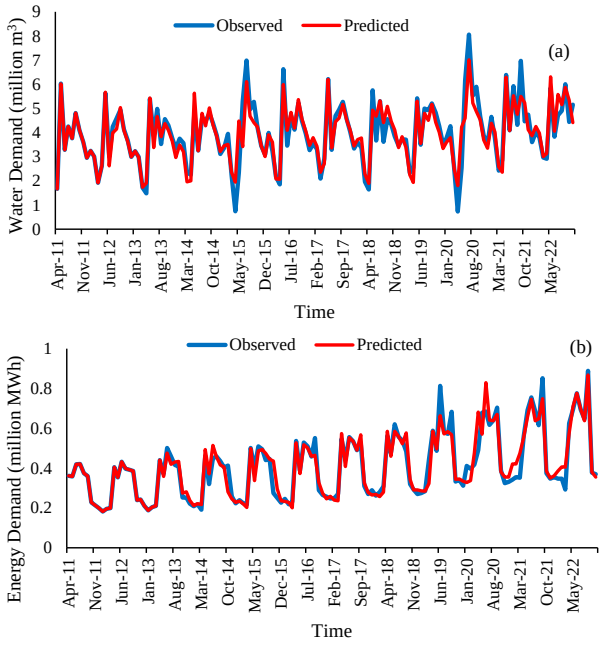


Figure 2. Results of forecasting (**a**) water demand and (**b**) energy demand from 2011 to 2022 in Yazd.

The results of metrics for forecasting water and energy demands are presented in Table 2. The metric results show that both SARIMA models performed well and provided relatively accurate predictions. Therefore, the predicted values can be utilized to forecast the future.

Table 2. Comparison of observed and predicted water and energy demands based on error metrics.

Demand	*RMSE*	*ME*	*MASE*	*NSE*	R^2
Water Demand	0.39	0.015	0.27	0.844	0.845
Energy Demand	0.28	−0.009	0.32	0.916	0.917

Using the SARIMA models with the most robust performances, water and energy demands from 2023 to 2032 in the city were forecasted (Figure 3). Furthermore, Figure 4 depicts that predicted water and energy demands have an upward trend. To be more precise, water consumption is expected to increase by 35% over the next decade compared to the past decade. Likewise, energy consumption will rise by approximately 77%. Due to the hot and dry climate and hot summers in Yazd, the highest water consumption occurs in the summer—approximately 25% more than in other seasons. Regarding energy

consumption, summer and spring consume twice as much energy as winter and autumn. These observations demonstrate that, without efficient management and planning for water and energy use, the city may face a crisis in supply during the summer. Therefore, future forecasting can significantly aid regional decision-makers in preventing such crises.

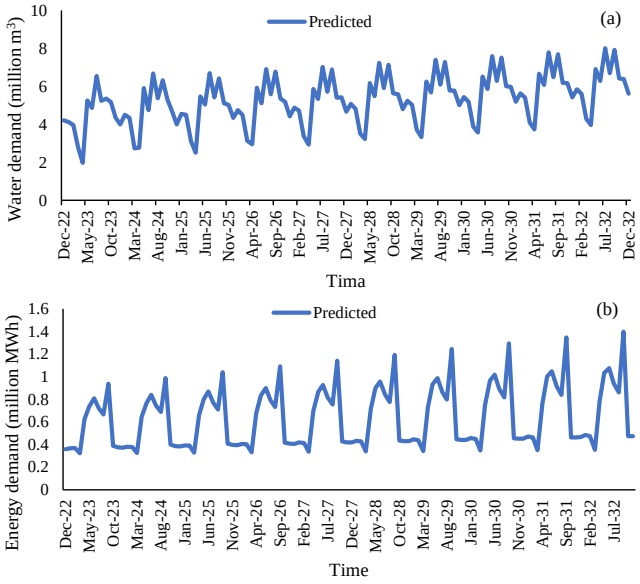


Figure 3. Results of future predictions of (**a**) water demands and (**b**) energy demands from 2023 to 2032 in Yazd.

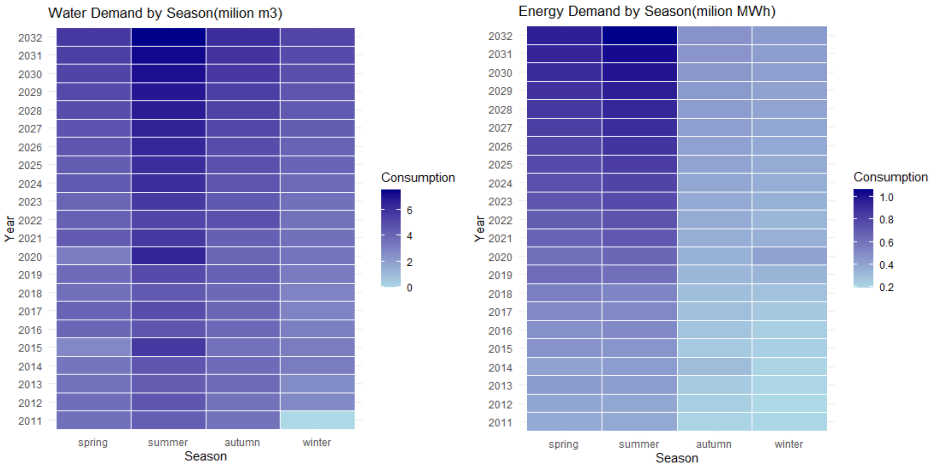


Figure 4. Variations in water and energy demands in different seasons from 2011 to 2032.

3.2. Copula Analysis Results

For monthly data from 2011 to 2023, the dependency between water and energy supply was examined. Table 3 shows that the Pearson correlation coefficient is 0.564, while Kendall's tau and Spearman's rho are 0.389 and 0.542, respectively. Based on the results shown in Table 3 and the scatter plot in Figure 5, there is a relatively strong positive relationship between the water and energy supply, making using copula a logical choice.

Table 3. Correlation coefficients between water and energy supply data.

Correlation Coefficient	Value
Pearson correlation coefficient	0.564
Kendall's tau	0.389
Spearman's rho	0.542

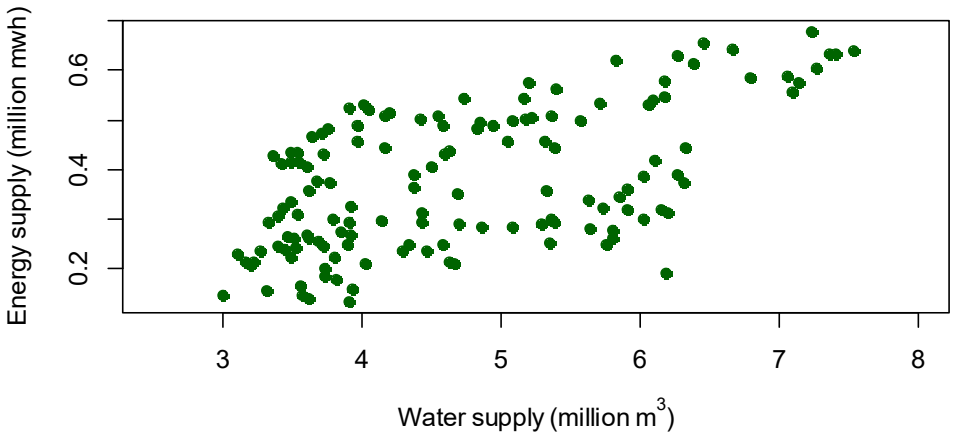


Figure 5. Scatterplot of water supply (million m^3) and energy supply (million MWh) from 2011 to 2022.

Suitable marginal distributions were fitted to the data, and an appropriate copula was selected. To this end, normal distribution and right-skewed distributions, including gamma, log-normal, and Weibull distributions, were considered due to the right-skewness of both datasets. Table 4 presents the parameters estimated by using maximum likelihood estimation (MLE), the KS statistic, AIC, and the *p*-value associated with the KS test for different distributions. According to Table 4, the log-normal distribution is the best fit for the water supply data, whereas the gamma distribution is the best fit for the energy supply data, as they have the lowest K-S statistic, the lowest AIC, and the highest log-likelihood values. Additionally, the *p*-value for the log-normal distribution for the water supply is 0.22, while the *p*-value for the gamma distribution for the energy supply is 0.32, indicating that the null hypothesis cannot be rejected at the 0.05 significance level for both distributions. Thus, the log-normal and gamma distributions fit the water and energy supply data well.

Figures 6 and 7 illustrate the fitted log-normal distribution for the water supply data and the gamma distribution for the energy supply data, respectively. According to Figures 6a and 7a, the red curve represents the theoretical density with which the data are compared. As shown, the density of the data is consistent with the density of the fitted distribution. Based on Figure 6b,d and Figure 7b,d, the data points follow a straight line of 45 degrees, and the fitting distribution is good. Furthermore, Figures 6c and 7c indicate that the empirical distribution of the data is compared with a theoretical one. As shown, the data are nearly on the red curve, which demonstrates that the specified marginal distribution fits the data well. Therefore, the log-normal and gamma distributions fit the water and energy supply data well.

Table 4. Fitted marginal distributions for historical data of water and energy supply (bold values provide better results).

Variables	Distribution	Estimated Parameters	Log-Likelihood	AIC	K-S Statistic	*p*-Value
Water supply	Normal	$\mu = 4.70$ $\sigma = 1.20$	204.15	−322.31	0.123	0.03
	Gamma	$\alpha = 14.96$ $\beta = 3.18$	222.83	−389.67	0.103	0.1
	Log-normal	$\mu_{lognorm} = 1.514$ $\sigma_{lognorm} = 0.266$	**259.24**	−414.93	**0.088**	**0.22**
	Weibull	$\alpha = 4.20$ $\beta = 5.16$	216.33	−356.67	0.113	0.06

Table 4. *Cont.*

Variables	Distribution	Estimated Parameters	Log-Likelihood	AIC	K-S Statistic	*p*-Value
Energy supply	Normal	$\mu = 0.38$ $\sigma = 0.14$	77.77	−151.55	0.105	0.09
	Gamma	$\boldsymbol{\alpha = 6.98}$ $\boldsymbol{\beta = 18.51}$	**85.84**	**−162.69**	**0.076**	**0.32**
	Log-normal	$\mu_{lognorm} = -1.04$ $\sigma_{lognorm} = 0.39$	78.69	−153.39	0.084	0.27
	Weibull	$\alpha = 2.98$ $\beta = 0.42$	80.76	−157.53	0.097	0.13

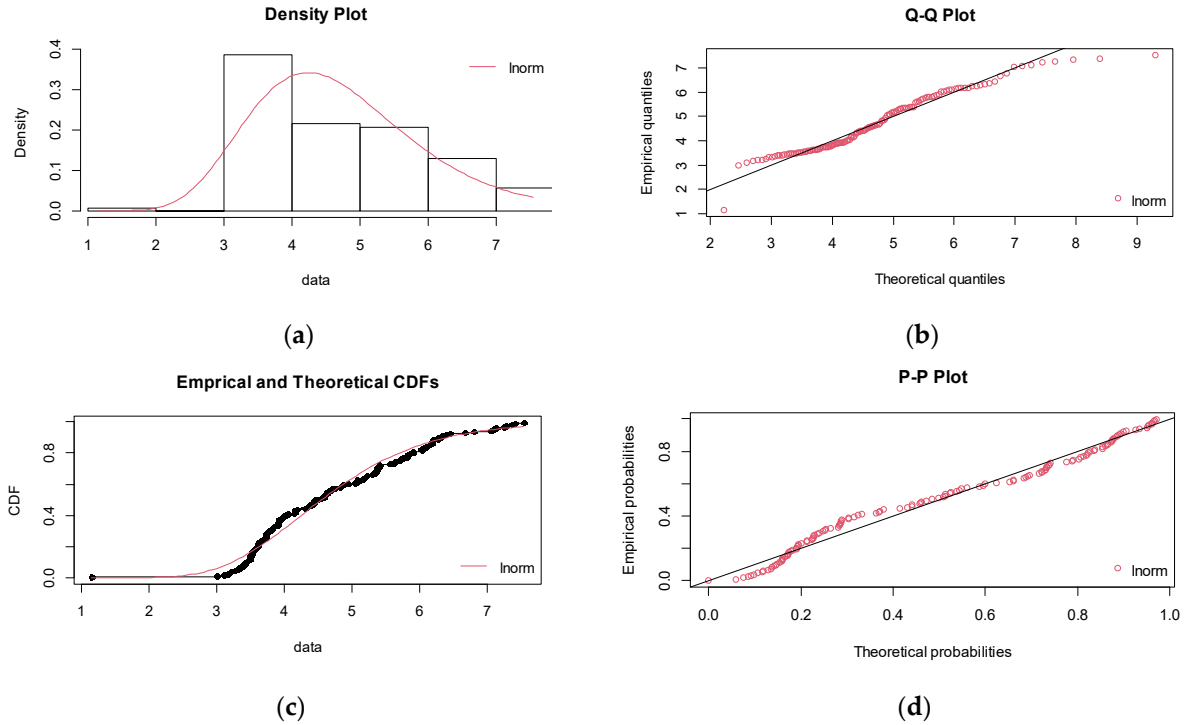


Figure 6. Goodness-of-fit plots for log-normal distributions fitted to the water supply data for historical data: (**a**) density plot, (**b**) Q-Q plot, (**c**) empirical and theoretical CDFs, and (**d**) P-P plot.

Figure 8 depicts the CDF for the historical water supply data. According to Figure 8, the probabilities for the water supply to be less than 5 million m^3 and less than 6.5 million m^3 are 0.64 and 0.91, respectively. Thus, when the water demand is 5 million m^3, the risk of water scarcity is 0.64. Additionally, the risk of water scarcity increases to 0.91 when the demand rises to 6.5 million m^3.

Figure 9 displays the CDF for the historical energy supply data. As shown, the probability is 0.82 when the energy supply is less than 0.5 million MWh and 0.93 when it is less than 0.6 million MWh. Therefore, when the energy demand is 0.5 million MWh, the risk of energy shortage is 0.82. As the demand increases to 0.6 million MWh, the risk of energy shortage increases to 0.93.

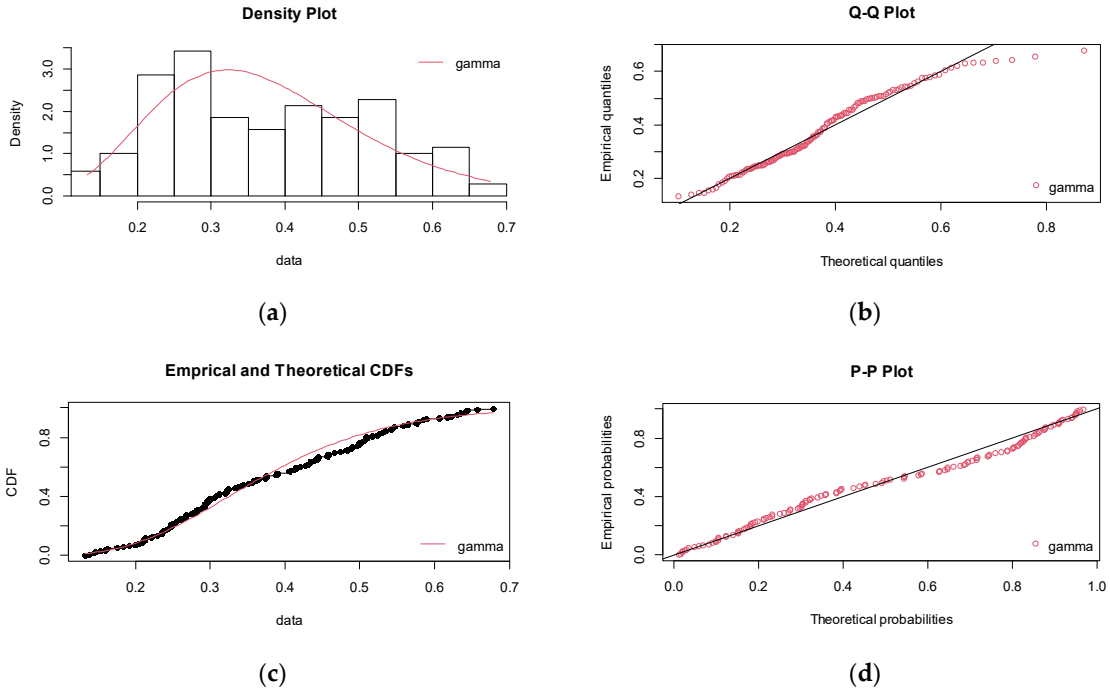


Figure 7. Goodness-of-fit plots for gamma distributions fitted to the energy supply data for historical data: (**a**) density plot, (**b**) Q-Q plot, (**c**) empirical and theoretical CDFs, and (**d**) P-P plot.

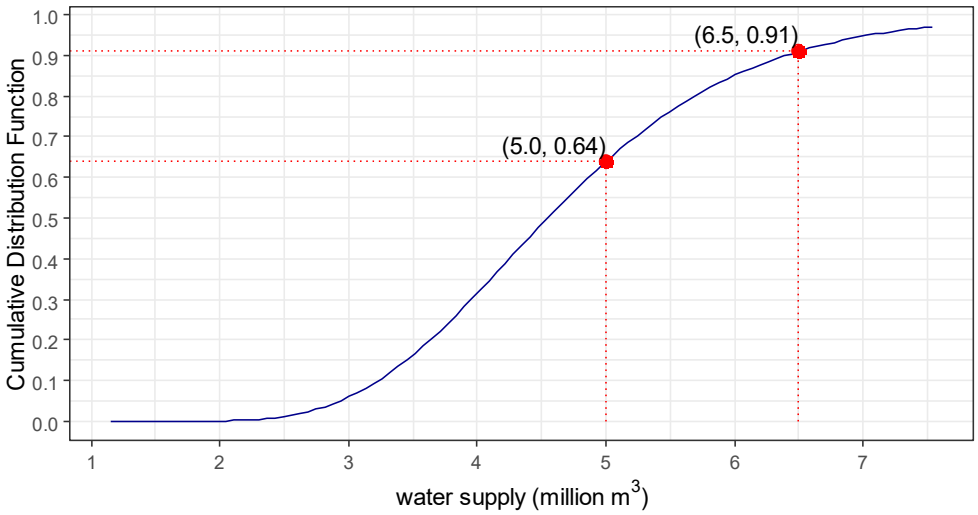


Figure 8. Cumulative distribution function of the water supply data from 2011 to 2022 in Yazd.

After transforming the data to a uniform distribution, the appropriate copula function was identified. For this purpose, commonly used copulas, such as Normal, t-Student, Gumbel, Clayton, and Frank, were considered. According to Table 5, the Gumbel copula has the lowest value of S_n, the lowest AIC value, and the highest log-likelihood value. Additionally, the p-value for the Cramér–von Mises test for this copula indicates that the null hypothesis is not rejected at a significance level of 0.05. Therefore, the Gumbel copula with a parameter of 1.66 is considered suitable for the data, and the data follow a bivariate distribution with Equation (23):

$$C_{\theta=1.66}(u,v) = \exp\left(-\left[(-lnu)^{1.66} + (-lnv)^{1.66}\right]^{\frac{1}{1.66}}\right) \quad (26)$$

where u is water supply, which follows a log-normal distribution, v is energy supply, which follows a gamma distribution, and θ is the Gumbel copula with a parameter of 1.66, as shown in Figure 10.

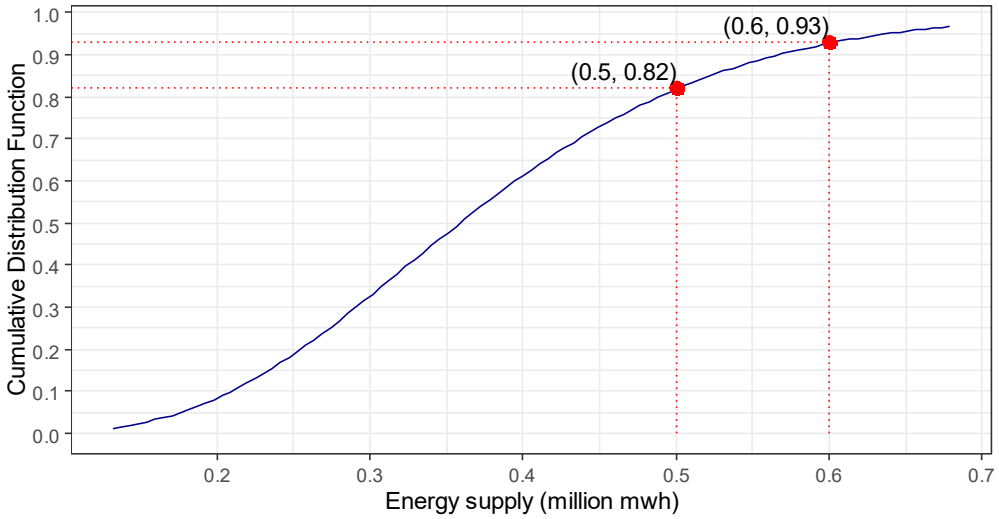


Figure 9. Cumulative distribution function of the energy supply data from 2011 to 2022 in Yazd.

Table 5. Fitted copula to the pairwise of historical data of water and energy supply (bold values provide better results).

Copula	Estimated Parameters	Log Likelihood	S_n	AIC	p-Value
Student-t	$\theta = 0.61$ $df = 59.10$	30.19	0.041	−56.38	0.02
Gumbel	$\boldsymbol{\theta = 1.66}$	**32.89**	**0.029**	**−63.78**	**0.10**
Clayton	$\theta = 1.27$	10.05	0.097	−18.09	0.00
Frank	$\theta = 3.81$	23.88	0.055	−45.76	0.00
Normal	$\theta = 0.61$	30.29	0.042	−58.58	0.01

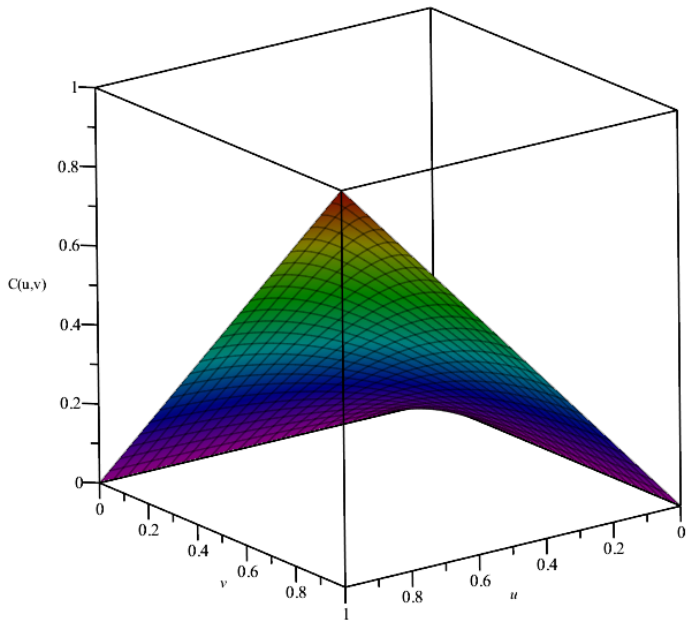


Figure 10. The Gumbel copula of water supply and energy supply.

3.3. Risk Analysis

Using the CDF charts and the relationship obtained between water and energy with the Gumbel copula function, the risk of water and energy supply in the future and the joint water–energy risk can be determined. The annual water and energy demand values from 2012 to 2022 were obtained from the relevant organizations. Using the SARIMA method, the water and energy demands from 2023 to 2032 were forecasted.

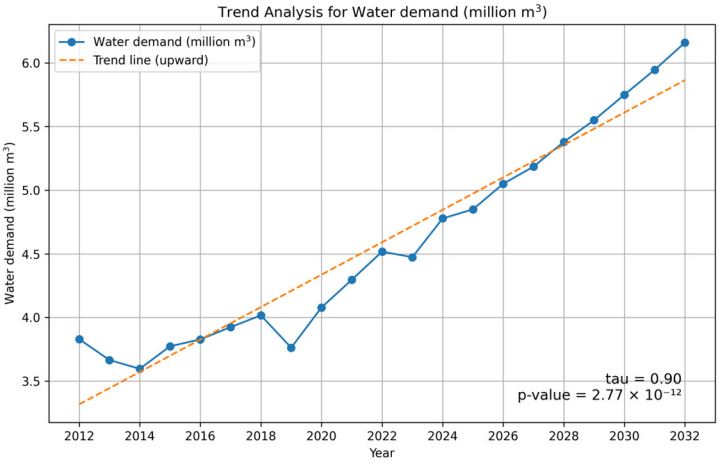
To calculate the risk of supplying each of water and energy demand, the distribution functions shown in Figures 8 and 9 were used for water and energy supply, respectively. For example, the water demand forecasted for 2023 is 4.473 million m^3. According to Figure 8, the probability of meeting this water demand is 0.48. Thus, the risk of water supply in 2023 is 0.48. The same process also applies to energy demands. For instance, the energy demand forecasted for 2023 is 0.558 Million MWh. According to the CDF shown in Figure 9, the probability that the energy supply will be less than or equal to 0.558 Million MWh is 0.89. Using the bivariate distribution function, the joint water–energy risk can also be calculated, which is 0.47 in 2023.

According to the results in Table 6, the risk of water supply in Yazd is projected to gradually increase, reaching 0.87 by 2032. The risk for energy supply is even more critical, expected to become 0.99 by 2032. This indicates a severe warning for the city. Based on the future predictions, Yazd will face a severe energy supply problem. Likewise, the risk of WEN is also expected to increase gradually, reaching 0.87 by 2032, based on Table 6. The results show that the risk of WEN is influenced by both water and energy values.

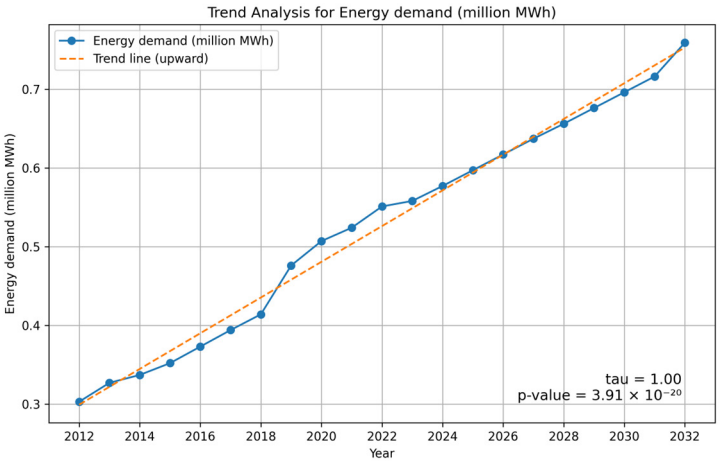
Table 6. Risk of water supply, energy supply, and water–energy nexus in Yazd.

Year	Water Demand (million m^3)	Energy Demand (million MWh)	Risk of Water Supply	Risk of Energy Supply	Risk of WEN
2012	3.829	0.303	0.26	0.33	0.16
2013	3.665	0.327	0.21	0.41	0.15
2014	3.596	0.337	0.19	0.43	0.14
2015	3.773	0.352	0.24	0.48	0.18
2016	3.827	0.373	0.26	0.54	0.21
2017	3.924	0.394	0.29	0.60	0.25
2018	4.016	0.414	0.32	0.65	0.28
2019	3.762	0.476	0.24	0.78	0.23
2020	4.078	0.507	0.34	0.83	0.33
2021	4.296	0.524	0.42	0.85	0.40
2022	4.517	0.551	0.49	0.88	0.48
2023	4.473	0.558	0.48	0.89	0.47
2024	4.778	0.577	0.57	0.91	0.56
2025	4.849	0.597	0.60	0.92	0.59
2026	5.050	0.617	0.65	0.94	0.65
2027	5.185	0.637	0.69	0.95	0.68
2028	5.379	0.656	0.74	0.96	0.73
2029	5.550	0.676	0.77	0.97	0.77
2030	5.750	0.696	0.81	0.97	0.81
2031	5.946	0.716	0.84	0.98	0.84
2032	6.160	0.759	0.87	0.99	0.87

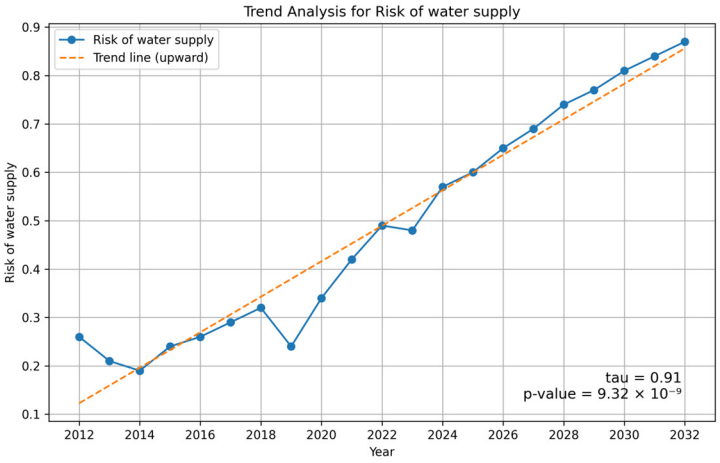
Mann–Kendall's test was applied to the forecasted water supply, energy supply, and water–energy nexus values presented in Table 6. As shown in Figure 11, water demand ($Z = 5.68$) and energy demand ($Z = 6.34$) forecasts indicate a significant upward trend (with p-values < 0.05) with a tau of 0.90 and 1.0, respectively. Additionally, the risk of water supply ($Z = 5.74$), energy supply ($Z = 6.31$), and WEN ($Z = 5.98$) are expected to have a significant upward trend with a tau of 0.91, 1.0, and 0.94, respectively, and p-values lower than 0.05. Therefore, the trend analysis demonstrates that the water and energy supply and their risk, in addition to the WEN risk, are expected to increase in the future in Yazd.



(**a**)

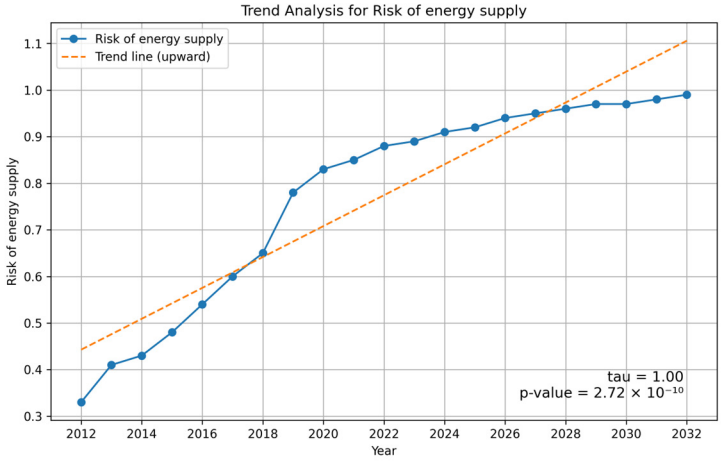


(**b**)

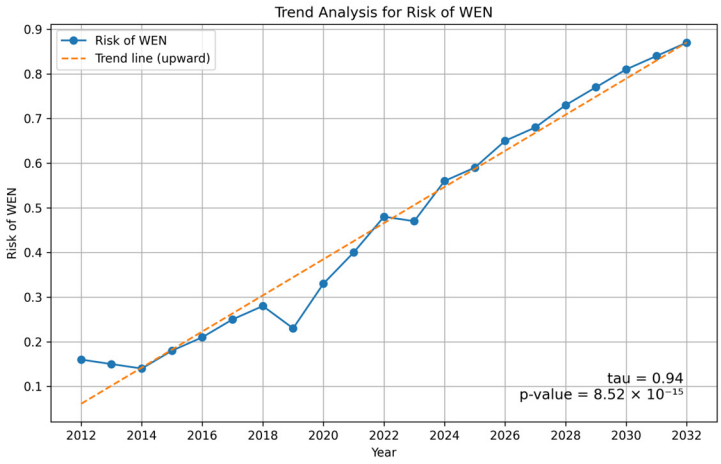


(**c**)

Figure 11. *Cont.*



(**d**)



(**e**)

Figure 11. Trend analysis results for the forecasted (**a**) water demand (million m^3), (**b**) energy demand (million MWh), (**c**) risk of water supply, (**d**) risk of energy supply, and (**e**) risk of WEN.

4. Discussion

Water and energy supply systems are consistently among the primary concerns for city officials. Urban managers continuously strive to meet the required amounts of water and energy using various methods while minimizing the risk of water and energy shortages. Since energy production also requires water consumption, water and energy inevitably influence one another. Identifying WEN can enable the simultaneous consideration of water and energy shortage risks. The current study used the copula function to examine and establish the relationship between the water and energy supply in Yazd. According to Table 6, the city is expected to face water and energy shortages in the future, particularly severe shortages for energy.

In this study, using the copula function, the relationship between the water and energy supply of Yazd was investigated. The results showed that in the future, this city could face a serious shortage of water and energy supply, especially in the energy sector. Also, the results of the copula function can be combined with other tools and concepts to achieve more useful results. For example, the scenario creation and two-level planning were used in addition to the copula results [49–51].

Also, copulas can serve as a tool to identify relationships among water, energy, and other factors. Earlier research primarily focused on scenario modeling and constructing hypothetical scenarios for the future.

This study, however, utilized existing data to forecast and evaluate past risks. To be more specific, SARIMA was employed to predict future water and energy demands. In previous studies, SARIMA was used to predict different values in dry areas. For example, Aghelpour et al. [52] compared the performance of SARIMA with those of other methods to predict future temperatures in several locations with different climates. The results showed that SARIMA has good results compared to other methods in dry areas. Legarreta-González et al. [53] also used SARIMA to estimate water consumption in Mexico, which has a hot and dry climate.

Therefore, the results of this study can serve as a warning to city managers that if they continue with the current approach, serious consequences may appear. To be more precise, without exploring alternative or supplementary sources for water and energy supply, the case study will likely encounter significant challenges in the future. Purification and reuse of wastewater for irrigation and the use of clean energy, such as solar and wind, are among the alternative ways that can be considered to reduce the risk to water and energy supplies.

Although city systems are highly complex with many influencing factors, considering more variables can lead to more accurate and realistic predictions. For instance, limitations of available water resources, restrictions on groundwater harvesting, population growth, and climate change are among the influencing factors that can affect the risk of water and energy supplies. This study did not consider the mentioned factors, but rather, it did consider other factors that may improve risk assessments in the future. As a result, future studies could incorporate additional factors, such as the environmental, economic, or even social aspects, and use multidimensional copulas to examine the relationships between these factors. Finally, data-driven approaches, like artificial intelligence, can be utilized in developing enhanced forecasting models in future works.

5. Conclusions

One of the primary concerns and responsibilities of city officials is meeting the criteria for the needs of water and energy supply. The study area (Yazd) is a city with a hot and arid climate that has always faced challenges in securing water, addressing this issue with various methods, such as water transfer. The energy needs of the city also encounter problems when consumption peaks in summer, leading to measures like power outages or changes in administrative working hours to reduce consumption. Therefore, estimating the risk of water and energy supply can help prevent crises by providing solutions before they occur.

Given that water is required for electricity production, it is obviously expected that water and electricity consumption will affect each other. Thus, considering these two variables together allows for a simultaneous assessment of water and energy supply risks.

Monthly water and energy consumption data from 2011 to 2022 were obtained from the local water and electricity authorities. Forecasting with the SARIMA method, water and energy consumptions from 2023 to 2032 were predicted. Metric results indicated that the developed models fit well with the existing data. To evaluate WEN, the correlation between water and energy supply data was examined using Pearson, Kendall, and Spearman correlation coefficients. The results demonstrated a relatively strong direct relationship between water and energy supply. Hence, the copula function was used to determine the relationship between water and energy supply in Yazd.

Initially, suitable marginal distributions were fitted to the data. Gamma, log-normal, and Weibull distributions were considered. For water supply data, the log-normal distribution and for energy supply data, the gamma distribution had the lowest K-S statistic, AIC value, and highest log-likelihood. Thus, the log-normal and gamma distributions fitted the water and energy supply data well, respectively. The CDF for water and energy was calculated and plotted. Using these plots and the estimated demand for water and energy supply from 2012 to 2032, the risks of water and energy supply were predicted. The results demonstrated that the risks for both water and energy supply will increase, with energy facing a more critical situation where the risk will reach 0.99 by 2032.

To calculate the simultaneous risk of water and energy supply, the copula function was fitted to the water and energy data. Various copulas, including normal, t-student, Gumbel, Clayton, and Frank, were considered. The Gumbel copula had the lowest Kramer–von Mises goodness-of-fit statistic, the lowest AIC, and the highest log-likelihood. Therefore, the Gumbel copula with a parameter of 1.66 was deemed suitable for the data, and the bivariate distribution relationship was obtained. As a result, the risk of WEN was calculated. Comparing the risks of water, energy, and WEN reveals that the risk of WEN will vary with changes in water and energy risks. The results for water, energy, and WEN risks indicate that the city will face a significant upward trend in water and energy demands and their separate and combined risks, which highlights a critical situation in the future.

By considering water and energy at the same time and the risk of their simultaneous supply, it is possible to provide more accurate forecasts and prevent the occurrence of a crisis. Nevertheless, there is uncertainty in other factors, like climate change or population increase, that can affect risk results. Due to data limitations in many areas, results of the model developed by available but limited data can be useful, while further parameters can be incorporated in the case of data availability. According to the results of this study, the copula function is a useful tool for identifying complex relationships between water and energy supplies. In addition, it can be utilized for the same purpose in other areas that have similar climate conditions. In future studies, multidimensional copula functions can be used to incorporate other parameters affecting the risk. Finally, other influential factors, such as climate change, population increase, water harvesting restrictions, and use of purified water for irrigation, can be considered, and their effects on risk can be evaluated in future studies.

Author Contributions: Conceptualization, M.R.G., S.A.-s.M., M.S. and M.N.; methodology, S.A.-s.M., M.S. and M.N.; software, S.A.-s.M.; validation, M.R.G., M.S., S.A.-s.M. and M.N.; formal analysis, S.A.-s.M., M.S. and M.N.; investigation, S.A.-s.M.; resources, M.S. and M.R.G.; writing—original draft preparation, S.A.-s.M., M.S. and M.N.; writing—review and editing, M.R.G. and M.N.; visualization, M.R.G. and M.N.; supervision, M.R.G. and M.N.; project administration, M.R.G. and M.N. All authors have read and agreed to the published version of the manuscript.

Funding: This research received no external funding.

Data Availability Statement: The data that support the findings of this study are available from the corresponding author upon reasonable request.

Conflicts of Interest: The authors declare no conflicts of interest.

References

1. Sawka, M.N.; Cheuvront, S.N.; Carter, R. Human water needs. *Nutr. Rev.* **2005**, *63* (Suppl. S1), S30–S39. [CrossRef] [PubMed]
2. Díaz-Caravantes, R.E.; Zuniga-Teran, A.; Martin, F.; Bernabeu, M.; Stoker, P.; Scott, C. Urban water security: A comparative study of cities in the arid Americas. *Environ. Urban.* **2020**, *32*, 275–294. [CrossRef]
3. Aljammaz, A.; Sultan, M.; Izadi, M.; Abotalib, A.Z.; Elhebiry, M.S.; Emil, M.K.; Abdelmohsen, K.; Saleh, M.; Becker, R. Land subsidence induced by rapid urbanization in arid environments: A remote sensing-based investigation. *Remote Sens.* **2021**, *13*, 1109. [CrossRef]
4. McLusky, D.; Elliott, M. *Transitional Waters: A New Approach, Semantics or Just Muddying the Waters?* Elsevier: Amsterdam, The Netherlands, 2007; pp. 359–363. [CrossRef]
5. Krugmann, H.; Goldemberg, J. The energy cost of satisfying basic human needs. *Technol. Forecast. Soc. Chang.* **1983**, *24*, 45–60. [CrossRef]
6. Savić, S.; Selakov, A.; Milošević, D. Cold and warm air temperature spells during the winter and summer seasons and their impact on energy consumption in urban areas. *Nat. Hazards* **2014**, *73*, 373–387. [CrossRef]
7. Goodarzi, M.R.; Mohtar, R.H.; Piryaei, R.; Fatehifar, A.; Niazkar, M. Urban WEF Nexus: An Approach for the Use of Internal Resources under Climate Change. *Hydrology* **2022**, *9*, 176. [CrossRef]
8. Hamiche, A.M.; Stambouli, A.B.; Flazi, S. A review of the water-energy nexus. *Renew. Sustain. Energy Rev.* **2016**, *65*, 319–331. [CrossRef]
9. Bozorgi, A.; Roozbahani, A.; Hashemy Shahdany, S.M.; Abbassi, R. Development of multi-hazard risk assessment model for agricultural water supply and distribution systems using bayesian network. *Water Resour. Manag.* **2021**, *35*, 3139–3159. [CrossRef]

10. Zeng, Y.; Liu, D.; Guo, S.; Xiong, L.; Liu, P.; Yin, J.; Wu, Z. A system dynamic model to quantify the impacts of water resources allocation on water–energy–food–society (WEFS) nexus. *Hydrol. Earth Syst. Sci.* **2022**, *26*, 3965–3988. [CrossRef]
11. Ahmadi, M.H.; Zarghami, M. Should water supply for megacities depend on outside resources? A Monte-Carlo system dynamics simulation for Shiraz, Iran. *Sustain. Cities Soc.* **2019**, *44*, 163–170. [CrossRef]
12. Hu, Z.; Wei, C.; Yao, L.; Li, L.; Li, C. A multi-objective optimization model with conditional value-at-risk constraints for water allocation equality. *J. Hydrol.* **2016**, *542*, 330–342. [CrossRef]
13. Wang, J.; Li, G.; Chen, H.; Liu, J.; Guo, Y.; Sun, S.; Hu, Y. Energy consumption prediction for water-source heat pump system using pattern recognition-based algorithms. *Appl. Therm. Eng.* **2018**, *136*, 755–766. [CrossRef]
14. De Amorim, W.S.; Valduga, I.B.; Ribeiro, J.M.P.; Williamson, V.G.; Krauser, G.E.; Magtoto, M.K.; de Andrade, J.B.S.O. The nexus between water, energy, and food in the context of the global risks: An analysis of the interactions between food, water, and energy security. *Environ. Impact Assess. Rev.* **2018**, *72*, 1–11. [CrossRef]
15. Yang, Y.; Wang, H.; Zhang, Y.; Wang, C. Risk assessment of water resources and energy security based on the cloud model: A case study of China in 2020. *Water* **2021**, *13*, 1823. [CrossRef]
16. Sun, C.; Wang, X.; Zheng, Y. An ensemble system to predict the spatiotemporal distribution of energy security weaknesses in transmission networks. *Appl. Energy* **2020**, *258*, 114062. [CrossRef]
17. Chen, L.; Huang, K.; Zhou, J.; Duan, H.-F.; Zhang, J.; Wang, D.; Qiu, H. Multiple-risk assessment of water supply, hydropower and environment nexus in the water resources system. *J. Clean. Prod.* **2020**, *268*, 122057. [CrossRef]
18. Chen, C.; Zeng, X.; Yu, L.; Huang, G.; Li, Y. Planning energy-water nexus systems based on a dual risk aversion optimization method under multiple uncertainties. *J. Clean. Prod.* **2020**, *255*, 120100. [CrossRef]
19. Cai, Y.; Cai, J.; Chen, D.; Xie, Y.; Feng, J. Development of an integrated prediction-optimization modeling approach for coupled risk management of water and energy nexus systems. *Sci. Total Environ.* **2021**, *781*, 146744. [CrossRef]
20. Alnahhal, Z.; Shaaban, M.F.; Hamouda, M.A.; Majozi, T.; Al Bardan, M. A Water-Energy Nexus Approach for the Co-Optimization of Electric and Water Systems. *IEEE Access* **2023**, *11*, 28762–28770. [CrossRef]
21. Kang, J.; Xu, L.; Ren, X.; Li, C.; Jia, Z.; Li, J.; Zhang, Y. An integrated assessment and prediction approach of water-energy nexus at the provincial scale: A case study of Inner Mongolia, China. *Energy* **2024**, *291*, 130438. [CrossRef]
22. Esmailpoor, N.; Esmaeilpoor, F.; Rezaeian, F. Explaining the causes of population outflow from the historical fabric of Yazd city. *Cities* **2023**, *137*, 104318. [CrossRef]
23. Pouriyeh, A.; Khorasani, N.; Hosseinzadeh Lotfi, F.; Farshchi, P. Efficiency evaluation of urban development in Yazd City, Central Iran using data envelopment analysis. *Environ. Monit. Assess.* **2016**, *188*, 618. [CrossRef] [PubMed]
24. Bozorg-Haddad, O.; Abutalebi, M.; Chu, X.; Loáiciga, H.A. Assessment of potential of intraregional conflicts by developing a transferability index for inter-basin water transfers, and their impacts on the water resources. *Environ. Monit. Assess.* **2020**, *192*, 40. [CrossRef] [PubMed]
25. Sadeghi, A.; Larimian, T.; Molabashi, A. Evaluation of renewable energy sources for generating electricity in province of Yazd: A fuzzy MCDM approach. *Procedia-Soc. Behav. Sci.* **2012**, *62*, 1095–1099. [CrossRef]
26. Goodarzi, M.R.; Vagheei, H.; Mohtar, R.H. The impact of climate change on water and energy security. *Water Supply* **2020**, *20*, 2530–2546. [CrossRef]
27. Scanlon, B.R.; Duncan, I.; Reedy, R.C. Drought and the water–energy nexus in Texas. *Environ. Res. Lett.* **2013**, *8*, 045033. [CrossRef]
28. Nouri, N.; Balali, F.; Nasiri, A.; Seifoddini, H.; Otieno, W. Water withdrawal and consumption reduction for electrical energy generation systems. *Appl. Energy* **2019**, *248*, 196–206. [CrossRef]
29. Sojoodi, S.; Dastmalchi, L.; Neshat, H. Efficiency ranking of different types of power plants in Iran using super efficiency method. *Energy* **2021**, *233*, 121104. [CrossRef]
30. Tang, T.; Xu, J.-Q.; Jin, S.-X.; Wei, H.-Q. Study on operating characteristics of power plant with dry and wet cooling systems. *Energy Power Eng.* **2013**, *5*, e656. [CrossRef]
31. Clark, C.E.; Horner, R.M.; Harto, C.B. Life cycle water consumption for shale gas and conventional natural gas. *Environ. Sci. Technol.* **2013**, *47*, 11829–11836. [CrossRef]
32. Kontopoulou, V.I.; Panagopoulos, A.D.; Kakkos, I.; Matsopoulos, G.K. A Review of ARIMA vs. Machine Learning Approaches for Time Series Forecasting in Data Driven Networks. *Future Internet* **2023**, *15*, 255. [CrossRef]
33. Niknam, A.R.R.; Sabaghzadeh, M.; Barzkar, A.; Shishebori, D. Comparing ARIMA and various deep learning models for long-term water quality index forecasting in Dez River, Iran. *Environ. Sci. Pollut. Res.* **2024**, *31*, 1–17. [CrossRef] [PubMed]
34. Alsharif, M.H.; Younes, M.K.; Kim, J. Time Series ARIMA Model for Prediction of Daily and Monthly Average Global Solar Radiation: The Case Study of Seoul, South Korea. *Symmetry* **2019**, *11*, 240. [CrossRef]
35. Parasyris, A.; Alexandrakis, G.; Kozyrakis, G.V.; Spanoudaki, K.; Kampanis, N.A. Predicting meteorological variables on local level with SARIMA, LSTM and hybrid techniques. *Atmosphere* **2022**, *13*, 878. [CrossRef]
36. Kibunja, H.W.; Kihoro, J.M.; Orwa, G.O.; Yodah, W.O. Forecasting precipitation using SARIMA Model: A case study of Mt. Kenya Region. *Math. Theory Model.* **2014**, *4*, 50–58.
37. Goodarzi, M.R.; Fatehifar, A.; Moradi, A. Predicting future flood frequency under climate change using Copula function. *Water Environ. J.* **2020**, *34*, 710–727. [CrossRef]
38. Liu, Z.; Guo, S.; Xu, X.; Xu, S.; Cheng, J. Application of Copula functions in hydrology and water resources: A state-of-the-art review. *Adv. Water Sci.* **2021**, *32*, 148–159.

39. Tenney, M.S. Introduction to Copulas. In *Enterprise Risk Management Symposium*; Mathematical Finance Company: Alexandria, VA, USA, 2003.
40. Cohen, I.; Huang, Y.; Chen, J.; Benesty, J.; Benesty, J.; Chen, J.; Huang, Y.; Cohen, I. Pearson correlation coefficient. In *Noise Reduction in Speech Processing*; Springer: Berlin/Heidelberg, Germany, 2009; pp. 1–4. [CrossRef]
41. Berger, V.W.; Zhou, Y. Kolmogorov–smirnov test: Overview. In *Wiley Statsref: Statistics Reference Online*; John Wiley & Sons, Inc.: Hoboken, NJ, USA, 2014. [CrossRef]
42. Cavanaugh, J.E.; Neath, A.A. The Akaike information criterion: Background, derivation, properties, application, interpretation, and refinements. *Wiley Interdiscip. Rev. Comput. Stat.* **2019**, *11*, e1460. [CrossRef]
43. Ziegel, E.R. *Statistical Inference*; Taylor & Francis: Abingdon, UK, 2002. [CrossRef]
44. Martynov, G. Cramer-von Mises Test for Gamma Familyof Distributions. ББК *22.17* Меж*43* **2021**, *47*, 55.
45. Hırca, T.; Eryılmaz Türkkan, G.; Niazkar, M. Applications of innovative polygonal trend analyses to precipitation series of Eastern Black Sea Basin, Turkey. *Theor. Appl. Climatol.* **2022**, *147*, 651–667. [CrossRef]
46. Niazkar, M.; Goodarzi, M.R.; Fatehifar, A.; Abedi, M.J. Machine learning-based downscaling: Application of multi-gene genetic programming for downscaling daily temperature at Dogonbadan, Iran, under CMIP6 scenarios. *Theor. Appl. Climatol.* **2023**, *151*, 153–168. [CrossRef]
47. Chicco, D.; Warrens, M.J.; Jurman, G. The coefficient of determination R-squared is more informative than SMAPE, MAE, MAPE, MSE and RMSE in regression analysis evaluation. *Peerj Comput. Sci.* **2021**, *7*, e623. [CrossRef] [PubMed]
48. Goodarzi, M.R.; Sabaghzadeh, M.; Barzkar, A.; Niazkar, M.; Saghafi, M. A comparison of machine learning methods for estimation of snow density using satellite images. *Water Environ. J.* **2024**, *38*, 437–449. [CrossRef]
49. Cai, Y.; Cai, J.; Xu, L.; Tan, Q.; Xu, Q. Integrated risk analysis of water-energy nexus systems based on systems dynamics, orthogonal design and copula analysis. *Renew. Sustain. Energy Rev.* **2019**, *99*, 125–137. [CrossRef]
50. Yu, L.; Xiao, Y.; Jiang, S.; Li, Y.; Fan, Y.; Huang, G.H.; Lv, J.; Zuo, Q.; Wang, F. A copula-based fuzzy interval-random programming approach for planning water-energy nexus system under uncertainty. *Energy* **2020**, *196*, 117063. [CrossRef]
51. Yu, L.; Li, Q.; Jin, S.; Chen, C.; Li, Y.; Fan, Y.; Zuo, Q. Coupling the two-level programming and copula for optimizing energy-water nexus system management—A case study of Henan Province. *J. Hydrol.* **2020**, *586*, 124832. [CrossRef]
52. Aghelpour, P.; Mohammadi, B.; Biazar, S.M. Long-term monthly average temperature forecasting in some climate types of Iran, using the models SARIMA, SVR, and SVR-FA. *Theor. Appl. Climatol.* **2019**, *138*, 1471–1480. [CrossRef]
53. Legarreta-González, M.A.; Meza-Herrera, C.A.; Rodríguez-Martínez, R.; Chávez-Tiznado, C.S.; Véliz-Deras, F.G. Time Series Analysis to Estimate the Volume of Drinking Water Consumption in the City of Meoqui, Chihuahua, Mexico. *Water* **2024**, *16*, 2634. [CrossRef]

Disclaimer/Publisher's Note: The statements, opinions and data contained in all publications are solely those of the individual author(s) and contributor(s) and not of MDPI and/or the editor(s). MDPI and/or the editor(s) disclaim responsibility for any injury to people or property resulting from any ideas, methods, instructions or products referred to in the content.